Applied Energy 377 (2025) 124614

Contents lists available at ScienceDirect

Applied Energy

journal homepage: www.elsevier.com/locate/apenergy

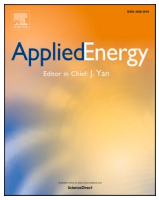

Real-time gas explosion prediction at urban scale by GIS and graph neural network

Jihao Shi [a], Junjie Li [a], Haoran Zhang [b,*], Bin Xie [c], Zonghao Xie [a], Qing Yu [b], Jinyue Yan [a]

[a] Department of Building Environment and Energy Engineering, The Hong Kong Polytechnic University, Hong Kong, China
[b] School of Urban Planning and Design, Peking University, Guangdong, China
[c] Gexcon China, Shanghai, China

HIGHLIGHTS

- A novel approach merges GIS with GNN for accurate urban-scale gas explosion prediction.
- Outperforms current machine learning and CFD methods in predicting gas explosion impacts.
- Introduces a real-time prediction model that considers complex urban geometries.
- Utilizes a comprehensive CFD-simulated dataset for robust GNN model training.
- Provides a decision-making tool for improving safety in the face of urban gas explosions.

ARTICLE INFO

Keywords:
Urban energy transition
Graph neural network
GIS
Urban scale gas explosion
Liquified natural gas

ABSTRACT

Liquified gases are expected to play the significant roles in the context of urban energy transition. However, the accidental release of liquified gases induces a flammable vapor cloud, almost 10 times larger than that of non-liquified gases. Its ignition in a congested urban block will result in even greater magnitudes of blast load, catastrophic for both structures and people at urban scale. Machine learning approaches have been developed to efficiently assess the consequence of gas explosion, while still having poor 。 performance to capture the interaction between congested buildings and blast wave propagation. This study aims to develop an integrated approach of Geographic information systems (GIS) and graph neural network (GNN), in which GIS provide 3D building geometries and grid information at urban scale. Computational fluid dynamics (CFD) simulation will be conducted to construct the benchmark dataset, by using which, the autoregressive GNN approach is developed to solve the interaction between congested buildings and blast wave propagation. Comparison with the existing machine learning-based prediction approaches is conducted. The results demonstrate our proposed approach has the higher R^2 value of 0.946 and lower *MSE* value of 5.36E-4, indicating its more accuracy to gas explosion evolution prediction especially at the congested urban areas. Our approach also exhibits 1000× computational speedup improvement compared to CFD approach at urban scale. This proposed approach has the potential to efficiently and accurately analyze the worst-case destructive effects of gas explosion at urban scale, supporting the decision-makings to improve urban resilience in the context of urban energy transition.

1. Introduction

Cities have become the significant contributors to global climate change, responsible for approximately 75 % of global CO2 emissions, stemming from transportation, energy consumption, industrial activities, and waste generation etc. [1]. However, cities also present an opportunity to implement impactful climate mitigation strategies and lead the way in transitioning to more sustainable practices [2,3]. Through the transition to cleaner energy sources, cities can actively work towards reducing their carbon footprint and combating climate change [4]. In the context of urban energy transition, the use of liquified gases such as liquefied natural gas (LNG) [5] or liquefied hydrogen (LH2) [6] can play a role in reducing emissions and transitioning to cleaner energy sources. These liquified gases can be used in urban areas

* Corresponding author.
E-mail address: h.zhang@pku.edu.cn (H. Zhang).

https://doi.org/10.1016/j.apenergy.2024.124614
Received 13 June 2024; Received in revised form 11 September 2024; Accepted 28 September 2024
0306-2619/© 2024 Elsevier Ltd. All rights are reserved, including those for text and data mining, AI training, and similar technologies.

for various applications including transportation, heating, and power generation. Their use can contribute to lowering greenhouse gas emissions and air pollution, thereby supporting the transition to more sustainable and environmentally friendly energy sources in urban environments [45]. Additionally, they can serve as a flexible energy source, complementing renewable energy technologies in the transition towards a more sustainable urban energy system [7,8].

The potentially applications pose additional safety concerns related to accidental release of liquified gas [9]. Once accidental release occurs, the liquified gas would evaporate with a very large volume expansion, resulting in a highly flammable vapor cloud covering a large-scale urban area with congested buildings. Compared to the non-liquified gases, igniting this large-scale flammable vapor cloud will lead to even greater magnitudes of overpressure, catastrophic for both structures and people around since the congested buildings can significantly enhance the evolution of gas explosion [10]. In 2023, an accidental release of LNG occurred from urban block in China and the released flammable vapor cloud rapidly spread to a very large area, causing a severe explosion and killing 38 casualties and damaging 4 nearby buildings [11]. In 2024, an accidental release of liquefied petroleum gas happened, and the released flammable vapor cloud quickly covers a range of several hundred meters. The subsequent explosion caused 5 casualties around [12].

Computational fluid dynamics (CFD) has become an accurate alternative to investigate gas explosion from urban block [13]. Zhao et al. [14] numerically investigated natural gas explosions in tunnels, and demonstrated the larger maximum overpressure induced by congested obstacles. Wang et al. [15] numerically studies natural gas explosion characteristics inside a building and found the numerically predicted loads were closed to that of real accident. The above studies focused on a specific building rather than block with congested buildings at urban scale, which could be affected by the accidental release of liquified gas. The integration of Geographic information systems (GIS) with CFD provides the alternative to investigate large-scale gas explosion with congested urban buildings [16]. Ma and Huang [17] conducted a quantitative risk analysis of a real-world urban gas station explosion accident by using GIS and CFD. Li et al. [18] applied ArcGIS software and CFD to numerically calculate the gas explosion risk distribution in coal mine. Mohr et al. [19] accurately predicted the effect of detonations at particular locations in urban environment by using GIS and CFD. Chen et al. [20] proposed the GIS-based approach to assess the real-time urban accidental consequences, and present the evaluated results for urban accidental decision-makings in 3D virtual environment. However, it is worthy noted that the integration of GIS with CFD approach is still computationally intensive for large-scale gas explosion prediction from urban block because of Navier-Stokes equations to be iteratively solved.

In order to solve this limitation, machine learning approaches have been applied to real-time gas explosion prediction with obstacles. Multilayer-perceptron (MLP) [21] and its derived approaches were commonly utilized to evaluate the gas explosion efficiently from factories, urban buildings, underground space [22,23]. In addition, Shi et al. [24] applied deep learning probability model to real-time predict spatial explosion overpressure of the offshore platform. Li et al. [25] developed Transformer neural networks for BLEVE loads prediction. However, the above machine learnings cannot model the interaction between buildings and gas explosion evolution, and thereby exhibit poor generalization to maximum overpressure prediction at urban area. Graph neural network (GNN) in this regard has the potential to handle with the fluid-structure interaction because of its powerful representation learning capability of between-node connections [26,27]. Gonzalez et al. [28] applied GNN to simulate the dynamics of complex systems by using graph node to represent the physical characteristic of each particle and graph edges to learn physical passing between the nearby particles. Peres et al. [29] integrated graph convolutional network with the differentiable fluid dynamics simulator to solve large complex partial differential equations. Li et al. applied GNN to predict the propagation of BLEVE overpressure wave [30]. However, as the authors' best known, few studies have investigated the GNN approach to gas explosion at urban scale with congested buildings.

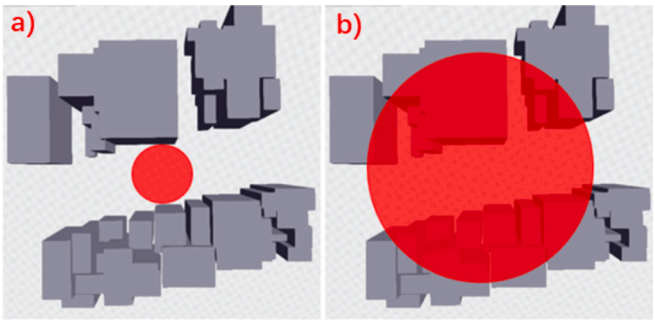

Fig. 1. Areas of flammable vapor cloud generated by non-liquified natural gas and liquified natural gas (LNG) in urban block. a) is that by natural gas release, b) is that by LNG release.

This study aims to develop an integrated approach of GIS and GNN for real-time gas explosion prediction at urban scale. This large-scale gas explosion may be caused during the expected widely applications of liquified gas such LNG and LH2 in the context of urban energy transition. In this proposed approach, GIS will provide the reliable 3D building geometries and grid information at urban scale. CFD simulation will be carried out to construct the numerical benchmark dataset. By using this dataset, the autoregressive GNN approach will be developed to solve the interaction between congested urban buildings and blast wave. Comparison with the state-of-the-art machine learning approaches is conducted to demonstrate the more accuracy of the proposed approach in terms of real-time prediction of large-scale gas explosion at urban scale. Destructive assessment of gas explosion at urban scale is conducted by using GIS and GNN approach, the higher efficiency of which is also analyzed compared to traditional GIS and CFD approach. The novelty and contributions are as follows:

1) An integrated approach of GIS and GNN is developed for real-time gas explosion at urban scale, in which GIS provides 3D urban building structures and GNN captures the interaction between urban buildings and blast wave.

2) A case study is conducted to demonstrate the higher accuracy and real-time capability of proposed approach to blast wave propagation prediction at urban scale compared to the state-of-the-art models of gas explosion prediction.

3) This developed approach has the potential to efficiently and accurately analyze the worst-case effects of gas explosion at urban scale, supporting the decision-makings about urban planning to improve urban resilience.

2. Problem formulation

Once the accidental release occurs, the liquified gases such as LNG or LH2 would evaporate with a very large volume expansion, resulting in a highly flammable vapor cloud covering a large-scale urban area with congested buildings. The subsequent explosion could cause the more severe destructive effect since the blast wave propagation would interact with more buildings at urban scale. Fig. 1 demonstrates urban areas covered by flammable vapor clouds generated by non-liquified gas and liquified natural gas (LNG) release. Fig. 1a) and Fig. 1b) are that by natural gas and LNG releases, respectively. From it, one may obviously see the larger area by LNG release covers more buildings compared to that by natural gas release. This is because the fast LNG evaporation could produce a flammable vapor cloud with approximated maximum distance of 100 m, almost 10 times larger compared to that by natural gas release [31,32].

Machine learning such as MLP and Transformer has been widely applied to analyze the gas explosion destructive effect. Its advantage is

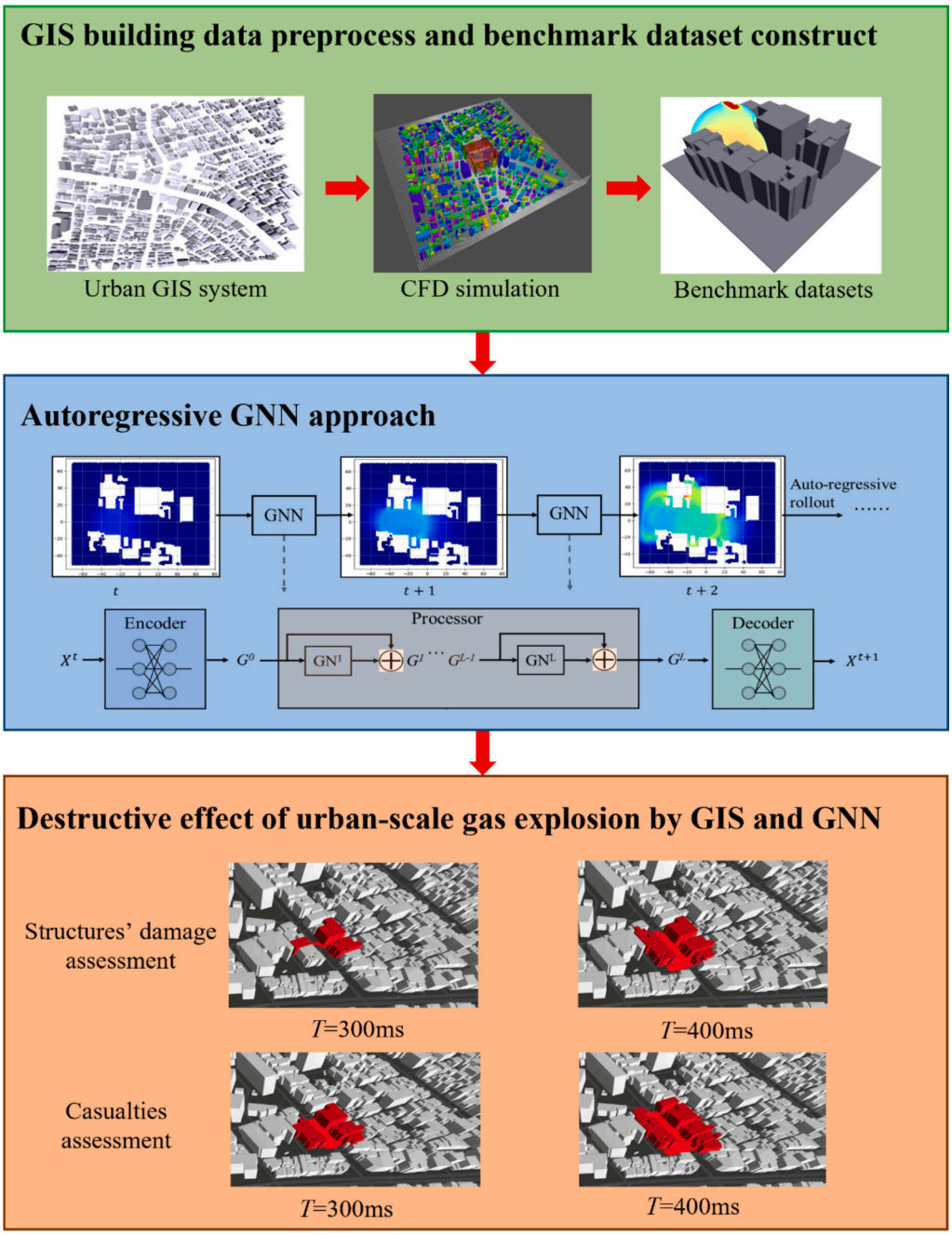

Fig. 2. Integration of GIS with the autoregressive GNN approach to real-time gas explosion prediction with congested buildings at urban scale.

the efficiency to determine the consequence of gas explosion, supporting the real-time decision-makings of accidental mitigation. However, the between-node dynamics of gas explosion, and the complex interaction between congested buildings and blast wave propagation are the significant factors on the destructive consequence. The existing machine learning-based approaches have the poor performance to capture the between-node dynamics of gas explosion, and the complex interaction between congested buildings and blast wave propagation. Such approaches thereby exhibit poor generalization to maximum overpressure prediction of obstructed gas explosion at urban scale.

Therefore, this study aims to apply the graph nodes to present the buildings and blast wave at specific area, and the graph edges to describe the interaction between buildings and blast wave. This described between-nodes dynamic has the potential to improve the accuracy of maximum overpressure prediction at urban scale with congested buildings. In addition, GIS will be integrated to provide the reliable 3D building geometries and grid information, which finally determines the initial graph structure of GNN approach. The prediction by GIS and GNN approach would support the efficient and accurate decision-makings to devise prevention and mitigation measures at urban scale so that accidental releases can either be prevented or their consequences can be minimized. It also supports urban planning so that densely populated areas are placed at a safe distance from the establishment where an accidental release could potentially happen in the context of urban energy transitions.

3. Methodology

This section introduces the integration of GIS with the autoregressive GNN approach to real-time large-scale gas explosion prediction with

congested buildings at urban scale. The 3D GIS building data will be preprocessed to construct 3D numerical geometry. The GIS grid configuration will be used for CFD numerical modeling. Subsequently, a large number of gas explosion simulations in large-scale urban block will be conducted. By using this numerical benchmark dataset, GNN approach with an autoregressive prediction scheme will be developed in which GIS grid configuration will be used. Also, we pre-define two constraint schemes to graph nodes corresponding to GIS building structures to determine the optimal one of presenting the interaction between congested buildings and blast wave.

3.1. GIS building data preprocess

The 3D GIS buildings data will be extracted from Mapbox, a location data platform designed for mobile and web applications. This GIS data consists of precise building footprints stored in GeoJSON format, in which each building object is defined by a polygon geometry that encompasses information concerning the building's outline contour and elevation. In this form of organization, the complex building structure being composed of multiple building modules with different heights is extracted. This extracted building data must undergo several preprocessing steps before being inputted into the CFD model and GNN development. These steps include:

Step 1: Converting the coordinates of the building data from the latitude and longitude geographic coordinate system to the projected coordinate system. This conversion ensures that the coordinates are represented in actual distance unit (meter *m* will be applied in this study).

Step 2: Constructing the building outline data into 3D objects that are compatible with the CFD numerical modeling. This step prepares the 3D building structure geometry for accurate CFD simulation.

Step 3: Creating a geographic grid configuration with equal distance intervals (0.5 m × 0.5 m in this study) based on the spatial range of the building. This grid configuration serves as the foundation for CFD numerical modeling as well as initial graph structure of GNN approach. Both the prepared 3D building structure geometry and grid information can be easily embedded to construct the numerical modeling by using pre-processing module of the well-known CFD software, i.e., FLACS.

Finally, a large number of gas explosion scenarios with congested urban buildings will be simulated by using CFD tool to construct the benchmark dataset for GNN approach development. This benchmark simulation data has the high accuracy to present the interaction between congested building and blast wave evolution, and thereby gas explosion prediction at large urban scale.

3.2. Autoregressive GNN approach

GNN approach with an autoregressive prediction scheme is applied to real-time simulate the gas explosion overpressure evolution with congested urban buildings. The initial graph structure is first generated by utilizing GIS grid data, building the spatial connections between GIS mesh points. In this graph structure, graph nodes and edges are applied to describe the between-node dynamics of blast wave evolution, and the interaction between buildings and blast wave. A spare and local graph edge at building-blast wave interface could be caused by the existence of urban buildings, which may inadequately represent the interaction between congested buildings and blast wave evolution. We thereby apply the well-known heuristic approach, namely kNN to solve this limitation [33]. In addition, both the GIS system and CFD numerical configuration have the graph nodes inside the 3D urban buildings. This induces the initial structure of GNN approach also contains such graph nodes. However, the reflection of blast wave by urban building surface causes them to be unable to pass through these building structures, indicating the graph nodes inside these buildings may have no effect on the blast wave evolution. This is to say the training process of GNN approach should ignore the effect of the predictions at the graph nodes inside these buildings on blast wave propagation. In this regard, we assume two schemes to predefine the constraint to these graph nodes inside these buildings to reduce the corresponding effect. The 1st constraint scheme, i.e., Scheme 1(rigid boundary condition) is to delete all the graph nodes inside these buildings indicating there will not be predictions at such graph nodes by the GNN approach. In addition, the 2nd constraint scheme, i.e., Scheme 2 (Hybrid Boundary Condition) fixes all the predictions at these graph nodes to be the initial values during training process. The 2nd scheme is similar with the CFD numerical boundary configuration at rigid buildings where all the physical parameters are fixed to be 0. Please noting that the difference between two constraint schemes lies in the loss function of GNN training process.

As is shown in Fig. 2, this GNN approach consists of three sections, namely encoder, processor and decoder. The encoder applies the fully-connected neural networks to encode the input X_t into the latent space, which can be expressed as $G^0 = Encoder(X_t)$. The input $X_t = \left[l_x, l_y, t, p_i^t\right]$ includes the coordinates (l_x, l_y) of the ith grid point, the maximum overpressure p_i^t at time t and the ith grid point. The latent space G^0 contains the transformed values at grid points and connections between the nearby grid points. In addition, the processor applies a GraphNet block [27] to provide the prediction by using the latent G^0 as input, which can be expressed as $G^1 = \text{GraphNet}\left(G^0\right)$. This prediction is iteratively conducted L times and finally the latent graph G^L is provided. During this iterative prediction process, both the embedded values at grid points and connections between the nearby grid points can be updated by using fully-connected neural networks. Subsequently, the decoder applies the fully-connected neural networks to give the final prediction given the latent G^L, which can be expressed as $X_{t+1} = Decoder\left(G^L\right)$ where X_{t+1} is the predicted maximum overpressures at time $t+1$ of all the grid points.

For the training process, the Scheme 1(rigid boundary condition) applies the mean square error (MSE) between the benchmark and predicted maximum overpressures of the grid points in the air domain as the loss function. The loss function of the Scheme 1 can be expressed as $LOSS(X_t, \theta) = MSE\left(Decoder\left(GraphNet(Encoder(X_t))_j - p_j^{t+1}\right)\right.$ where θ presents the hyperparameters such as weights and biases of neural networks, and j presents the jth grid point in the air domain. In addition, the Scheme 2 applies the mean square error (MSE) between the benchmark and predicted maximum overpressures in the air domain as the 1st term of loss function, and fixes the predicted maximum overpressures inside these buildings to be 0. The loss function of Scheme 2 can be expressed as $LOSS(X_t, \theta) = MSE\left(Decoder\left(GraphNet(Encoder(X_t))_j - p_j^{t+1}\right)\right. + MSE\left(GraphNet(Encoder(X_t))_z - 0\right)$ where z is the zth grid point inside these buildings.

By using the training dataset, AdamW optimizer [34] is applied to determine the optimal hyperparameters. Gaussian noise is added into the training data to effectively avoid the substantial increase in error accumulation of autoregressive prediction [28,35,36]. The validation dataset is then applied to evaluate the generalization of GNN approach to unseen explosion scenarios. The GNN model which has the lowest validation error is applied for comparisons with the state-of-the-arts by using testing dataset. Once the optimal one after the final testing is determined, this developed GNN approach will be incorporated into GIS system to assess the destructive effect of gas explosion on surrounded structures and people at urban scale. This will support the decision-makings to devise prevention and mitigation measures at urban scale and also supports urban planning so that densely populated areas are placed at a safe distance from the establishment where an accidental release could potentially happen in the context of urban energy transitions.

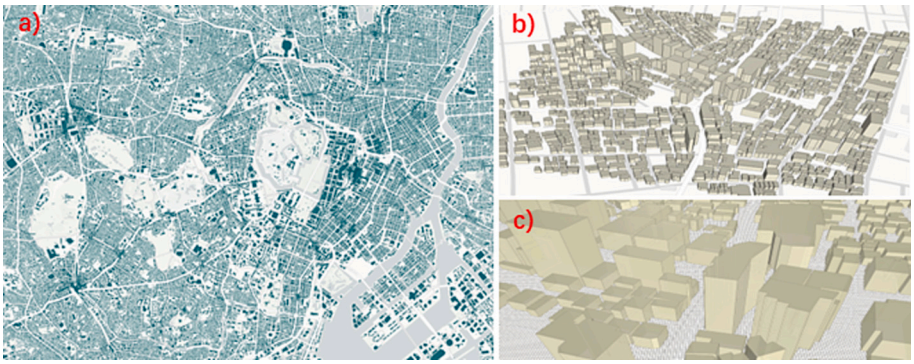

Fig. 3. 3D GIS building and grid information in Tokyo Area of Japan.

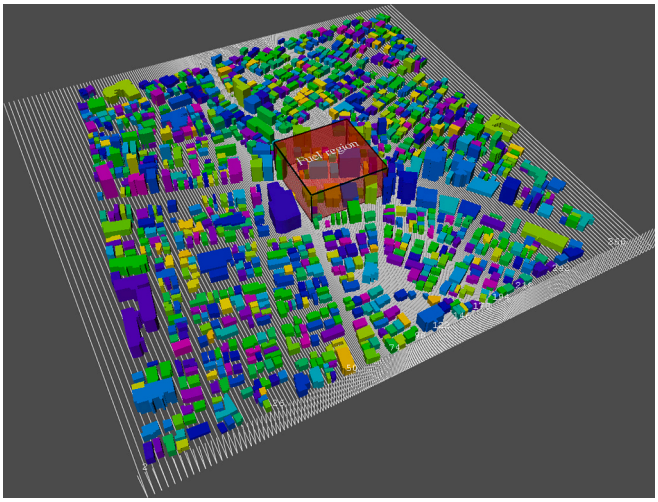

Fig. 4. Numerical modeling of gas explosion from large-scale congested urban block with dimensions of 500 m × 500 m by using FLACS.

4. Numerical benchmark datasets

4.1. Numerical modeling

The building GIS data including 3D building structures and grid configuration in the Tokyo Area of Japan as is shown in Fig. 3 is used in this case study. Fig. 3a) is the GIS data of Tokyo Area of Japan, Fig. 3b) shows 3D building structures at urban scale with dimensions of 500 m × 500 m, and Fig. 3c) demonstrates the local map grid cells, the size of which is 0.5 m.

The 3D building structures at urban scale with dimensions of 500 m × 500 m in Fig. 3b) are used as urban block geometry for CFD numerical modeling and simulation. The CFD software, namely FLACS, which has been widely experimentally validated in terms of gas explosion from offshore facilities [37], large-scale twin-compartment [38], urban shallow buried pipe trenches [39], hydrogen storage chamber [40], LNG tank [41], and BLEVE [30], is applied in this study. In addition, the authors recently experimentally validated its accuracy to overpressure prediction of gas explosion from offshore rig [24]. FLACS applies k-ε turbulence model and b-flame model to present the coupling effect between building-inducing turbulence generation and flame propagation. Based on the accurately modeling of turbulent flame propagation, FLACS can simulate the spatiotemporal evolution of gas explosion blast wave over congested urban buildings.

Fig. 4 demonstrates the numerical gas explosion modeling from large-scale congested urban block with dimensions of 500 m × 500 m. The whole numerical domain covering this large-scale urban block has the dimensions of 500 m in X, 500 m in Y and 40 m in Z, respectively. The numerical domain is divided into two parts, namely the core and expansion numerical domains. The core domain is assumed to cover the selected urban block including a main road, reflecting the urban layout where gas pipeline of often follow its route. Within this core domain, a flammable vapor cloud is configured, measuring 100 m × 100 m × 40 m, designed to encompass the buildings in the area. This configuration is based on references [31, 32] and assumes that the release and dispersion of LNG at the urban scale are not part of this study. The chosen configuration of the flammable vapor cloud is intended to simulate a worst-case scenario for a gas explosion at the urban scale. The developed GNN model would be suitable to conduct the real-time conservative assessments of such worst-case gas explosion scenarios. According to the GIS grid configuration and FLACS manual recommendation [42], the

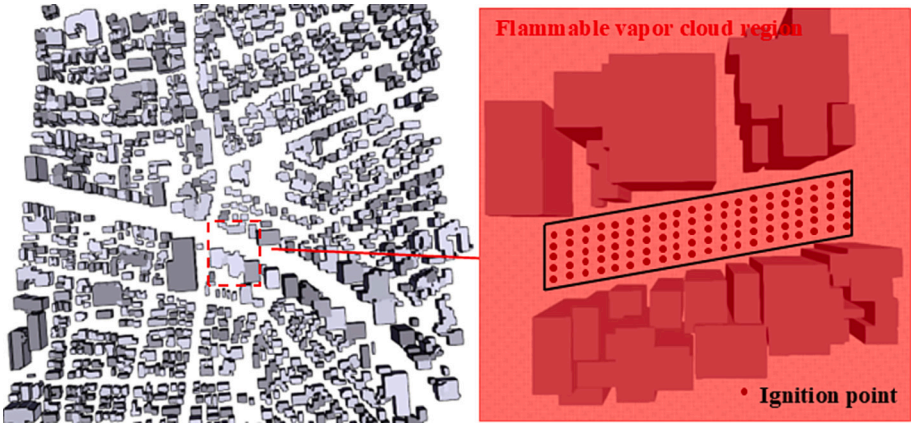

Fig. 5. Ignition region including 100 ignition points, which are evenly distributed along the main street, with a spacing of 0.15 cm vertically and 0.3 cm horizontally.

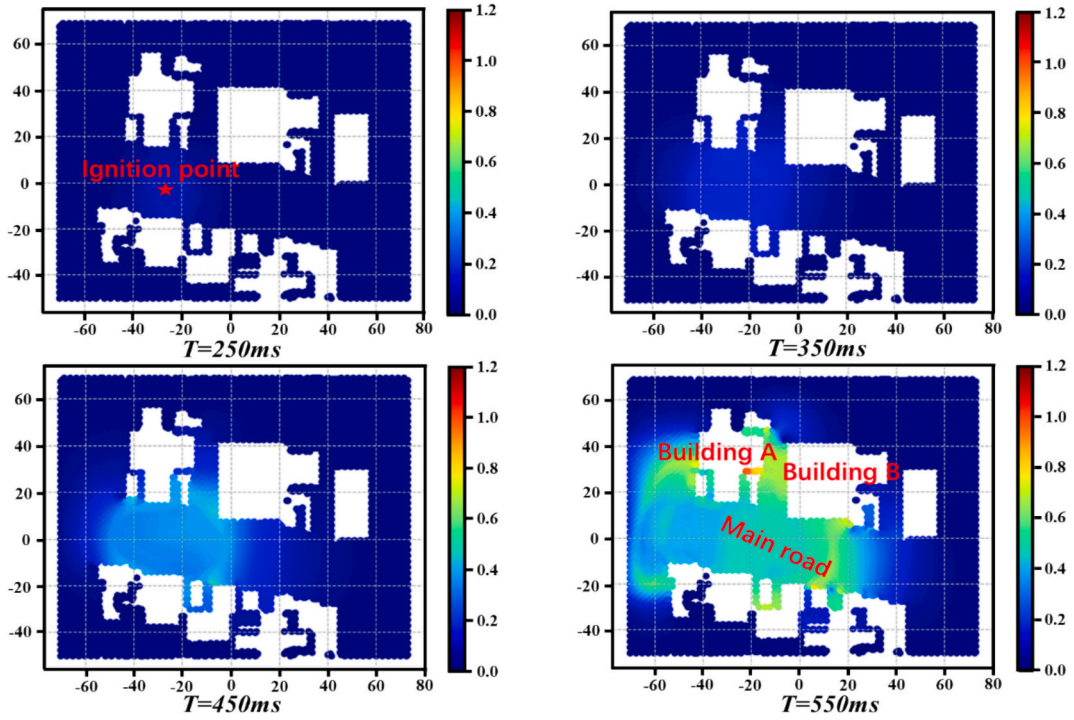

Fig. 6. Benchmark spatiotemporal evolution of maximum overpressure at time t=250 ms, 350 ms, 450 ms and 550 ms, respectively, under ignition point (x = −30, y = 0) from test dataset.

uniform grid-cell with 0.5 m is adapted in the core domain and an factor of 1.05 is applied to extend the grid of core domain to cover the entire numerical domain including its boundaries, resulting in a total of 7,560,000 grid cells. This will significantly reduce the computational costs while ensuring the simulation convergency. Wall boundary condition is used in terms of 3D building geometry. An open boundary condition is applied to the whole numerical domain to minimize its reflection effect on blast wave in the core numerical domain. The time step criterion is CFLC = 5, CFLV = 0.5, representing 5 control units for acoustic wave propagation, and 0.5 control units for fluid propagation at this time. By using the constructed numerical model, we consider 100 ignition points following the main road in the core domain, indicating we totally simulate 100 scenarios of gas explosion. Fig. 5 shows the region of flammable vapor cloud and ignition region including 100 points, which are evenly distributed along the main street, with a spacing of 0.15 cm vertically and 0.3 cm horizontally.

4.2. Benchmark dataset preprocessing

The duration of each simulation is 550 ms and the interval for writing the simulation results is set to be 10 ms. This means that the simulation captures and records the state of the system at every 10 ms interval throughout the duration of 550 ms, providing spatiotemporal simulation results. For each explosion scenario, we extracted the maximum overpressure data $x_i = [l_x, l_y, t, p_i^t]$. at the height z = 2.35 m where both l_x and l_y are from 0 m to 100 m with 0.5 m intervals, t is from 0 ms to 550 ms with 10 ms interval. Totally, we collect the benchmark dataset $100x_i$ for GNN approach development. We consider $[l_x, l_y, p_i^t]$ at time t as the input and $[l_x, l_y, p_i^{t+1}]$ at subsequent time $t+1$ as the output. We randomly divide the dataset into two sets, namely training set D_{train} (80 %), validation set D_{val} (10 %) and testing set D_{test} (10 %). In addition, the efficiency of our developed GNN approach depends on using preceding maximum overpressures to predict that of subsequent steps. This autoregressive prediction will unavoidably cause the accumulated prediction error over time. To address this, we inject noise data following by a Gaussian distribution with mean 0 and standard deviation σ to training data. Noting that this standard deviation (σ) will be linearly increased from 0 to 0.05, starting at the initial time step and ending at the final step. Following noise injection, we normalize both input and output maximum overpressure vectors, ensuring the values of each vector are between 0 and 1.

5. Model development, validation and comparison

5.1. Model development

The architecture of proposed GNN approach is compiled by using an open-source environment, i.e., PyTorch and PyTorch Geometric. A computing server with 64GB RAM, Intel (R) CoreTM i9-9900K CPU, and an NVIDIA GeForce RTX 2080 Ti GPU card is used for the development, validation and comparison of GNN approach. The GNN architecture can be seen in Appendix A.

We first select the benchmark simulation result under ignition point (x = −30, y = 0) from test dataset as the example to analyze the optimal one between two predefined constraint schemes. Please noting that this selected ignition point represents the edge ignition conditions of the whole numerical domain under which the blast wave propagation along one direction of the main road could interact with more building structures. Fig. 6 displays the benchmark spatiotemporal evolution of maximum overpressure at time t=250 ms, 350 ms, 450 ms and 550 ms, respectively. This benchmark sequence is selected from testing dataset. Fig. 7 a) and Fig. 7 b) are the predictions by GNN approach under constraint scheme 1 and constraint scheme 2, respectively. From it, one may see the GNN approach under constraint scheme 1 predicts the spatiotemporal evolution of maximum overpressure very closed to the benchmark data before the blast wave approaches the building surfaces, i.e., before 350 ms. After that, the blast wave interacts with the building surfaces, which enhances the maximum overpressures closed to the congested buildings. At T = 550 ms, because of the constraint effect by the building A and building B, one may see the larger maximum overpressures are distributed at this area between building A and building B. The GNN approach under constraint scheme 1 can accurately predict

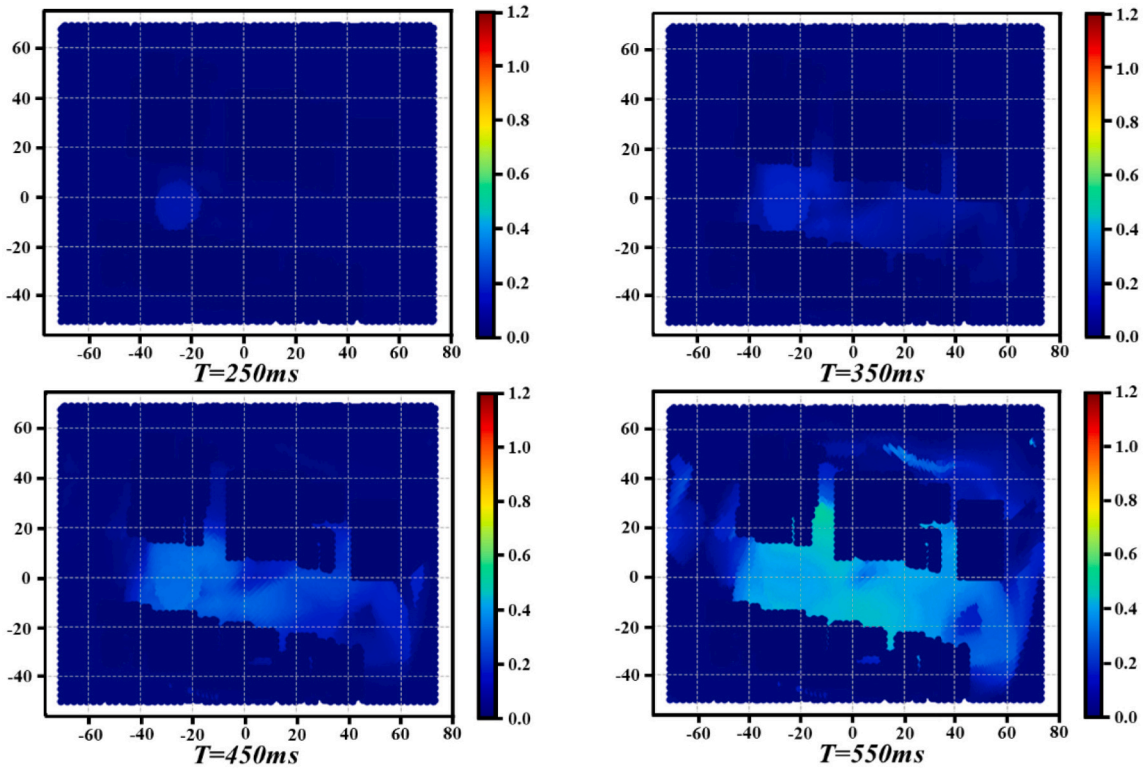

a) GNN approach under constraint scheme 1

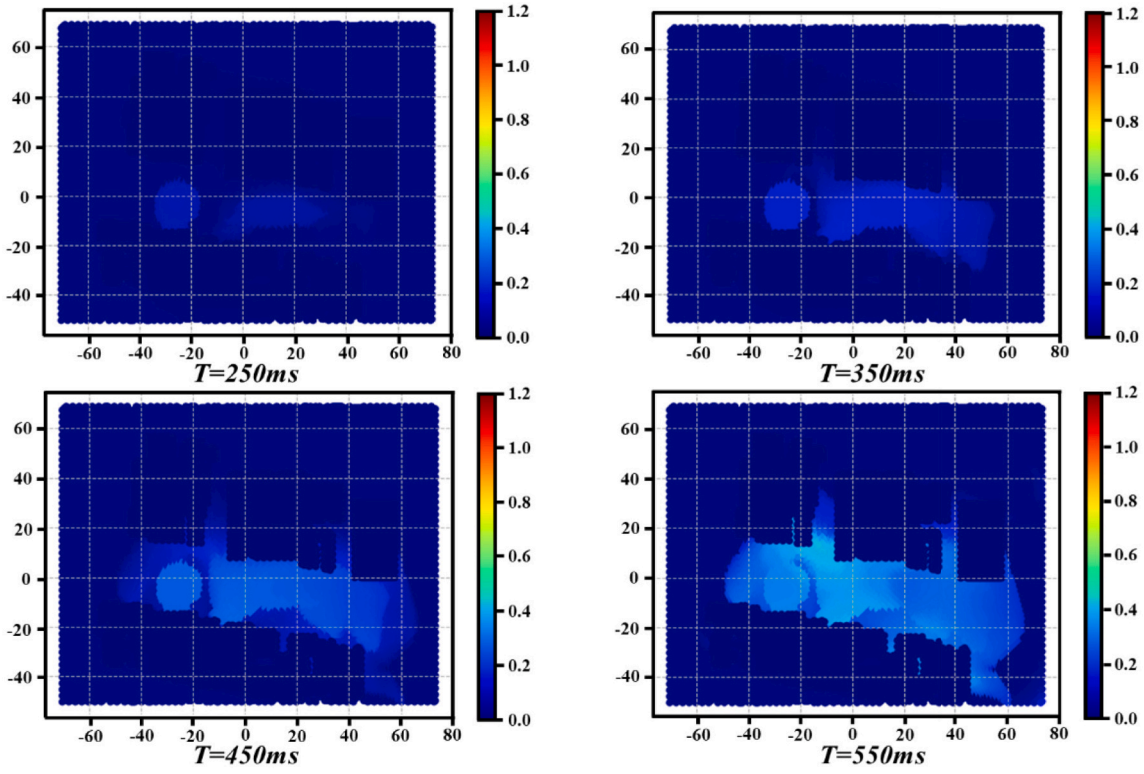

b) GNN approach under constraint scheme 2

Fig. 7. Spatiotemporal evolution of maximum overpressure predicted by GNN approach under 2 constraint schemes at time t=250 ms, 350 ms, 450 ms and 550 ms, respectively. Noting that ignition point (x = −30, y = 0) is same with that of Fig. 6.

Table 1
Comparison of R^2 and *MSE*.

Model	R^2	*MSE*
Without considering blocks	0.9460	5.36E-4
Considering blocks	0.5322	1.86E-3

these larger maximum overpressures enhanced by buildings. However, the developed GNN approach under constraint scheme 2 can only predict the higher overpressures along the main road between buildings. Significant differences exist between the predictions by GNN approach under constraint scheme 2 and benchmark data at the area between building A and building B. This indicates the GNN approach under constraint scheme 1 has the more accurate performance to describe the effect of interaction between buildings and blast wave on the spatiotemporal evolution of maximum overpressure.

Table *1* demonstrates comparison of Root Mean Square Error (*RMSE*), and Coefficient of Determination (R^2) between 2 constraint schemes of developed GNN approach. Please noting that both R^2 and *MSE* values are determined by using all the simulation data from testing dataset. From it, one may see the developed GNN approach under constraint scheme 1 has the higher R^2 value and lower *MSE* value compared to that under constraint scheme 2 This indicates the more accuracy of GNN approach under constraint scheme 1 in terms of gas explosion prediction with congested buildings at urban scale.

5.2. Validation and comparison

The developed GNN approach under constraint scheme 1 is applied to compare with the state-of-the-art approaches, namely MLP and Transformer in terms of gas explosion prediction with congestions. Both architectures of MLP and Transformer are adopted from the references [43, 44], and the details can be seen in Appendix A. Also, we provide summarized table of optimization hyperparameters of MLP, Transformer and the developed GNN for the following comparative analysis in Appendix A. For both the MLP and Transformer models, the input includes relevant physical parameters that influence the overpressure, such as the spatial coordinates of the grid cells, and the historical maximum overpressure data at each grid point. Both models are trained on a dataset of known overpressure values from the high-fidelity FLACS simulations. Once being trained, both models can be used to make real-time predictions of the maximum overpressure at a given set of grid cell coordinates, using the historical overpressure data as input.

We first select the benchmark simulation result under ignition point (x = 0, y = 0) from test dataset as the example. Please noting that the ignition point with (x = 0, y = 0) represents the middle ignition conditions of the whole numerical domain under which the blast wave propagation along one direction of the main road would be affected by less building structures. Fig. 8 displays the benchmark spatiotemporal evolution of maximum overpressure at time t=250 ms, 350 ms, 450 ms and 550 ms, respectively. This benchmark sequence is selected from testing dataset and its ignition position is (x = 0, y = 0). Fig. 9a), b) and c) show the corresponding predictions by GNN, MLP and Transformer approaches, respectively.

From Fig. 8, one may see before T = 350 ms, the blast wave of gas explosion does not approach the building surfaces. Without the interaction with congested buildings, the blast wave induces relatively lower maximum overpressures. However, after time T = 450 ms, one may obviously see the increase of maximum overpressures especially closed to the building surfaces at for example the area between building A and building B, at area between building B and building C, and Area1. This is because the confined area between two buildings can enhance the blast wave propagation and thereby increase the maximum overpressure. From Fig. 9a), one may see our developed GNN approach predicts the distribution of maximum overpressure similar with the benchmark data before T = 350 ms. After T = 350 ms, our developed GNN approach predicts higher values of maximum overpressure at the corresponding area between building A and building B, area between building B and building C, and Area1, even though the very limited differences between predicted values and benchmark values of these areas still exist. From Fig. 9b), it can be seen that the distributions of maximum overpressure by the MLP approach at different time are different from that of

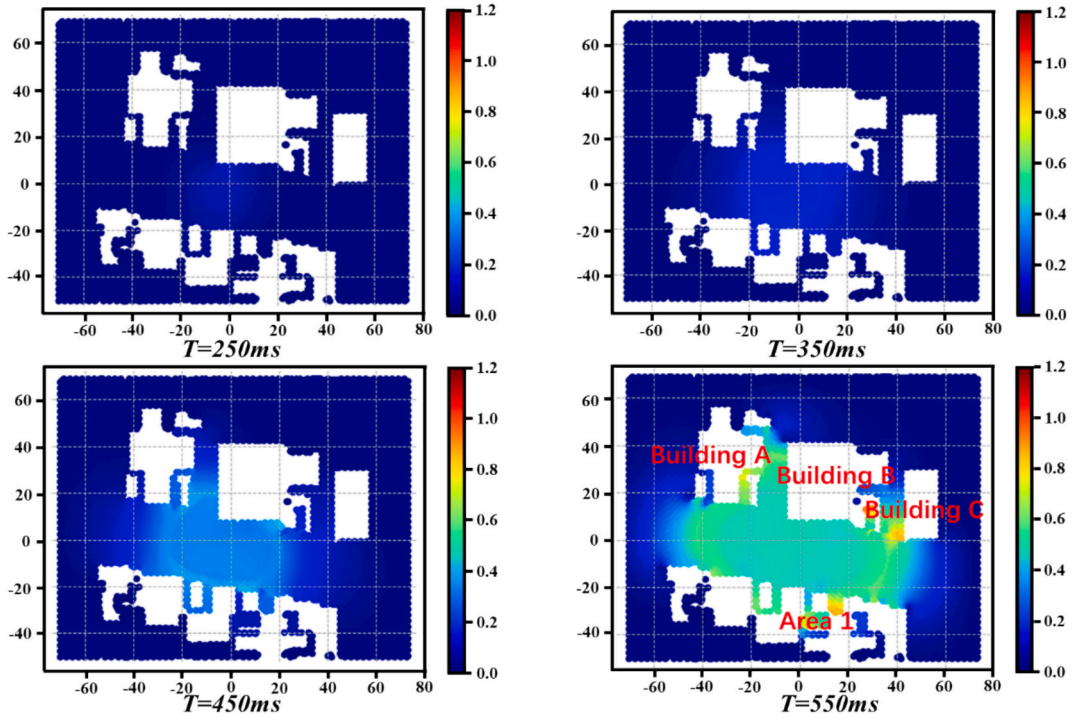

Fig. 8. Benchmark spatiotemporal evolution of maximum overpressure at time t=250 ms, 350 ms, 450 ms and 550 ms, respectively, under ignition point (x = 0, y = 0) from test dataset.

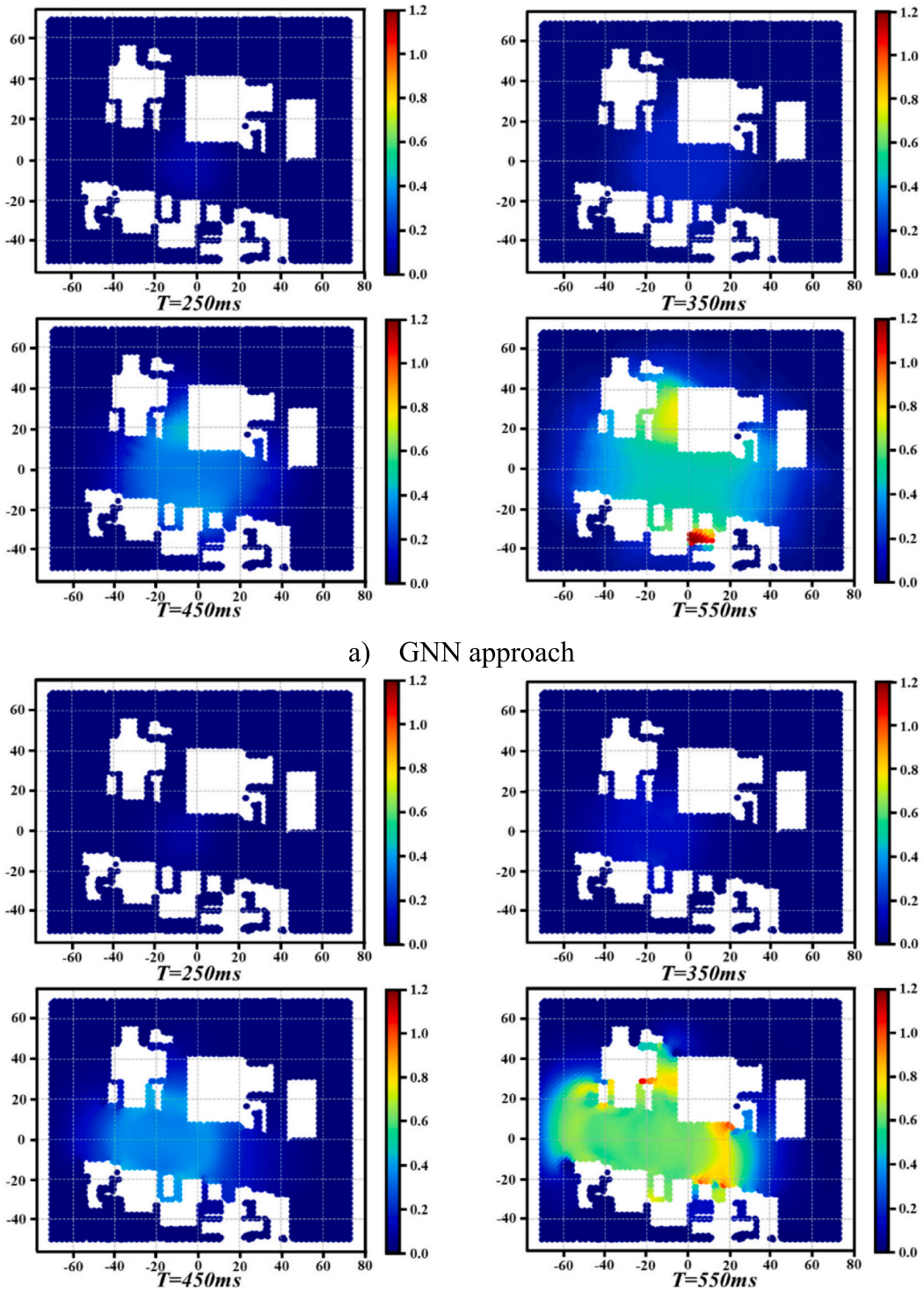

Fig. 9. Spatiotemporal evolution of maximum overpressure predicted by GNN, MLP, and transformer approaches at time t=250 ms, 350 ms, 450 ms and 550 ms, respectively. Noting that ignition point (x = 0, y = 0) is same with that of Fig. 8.

benchmark data even though the larger maximum overpressures at for example area between building A and building B can be predicted. This indicates the bad performance of MLP approach to present the constraint effect on blast wave propagation of gas explosion with congested buildings. Furthermore, from Fig. 9c), one may see the Transformer approach gives the more accurate predictions before T = 450 ms in terms of the distributions of maximum overpressure compared to the MLP approach. However, at T = 550 ms, the predicted values of maximum overpressures are relatively lower at the confined areas such as the area between building A and building B, at area between building B and building C, and Area1. This also indicates the Transformer approach cannot accurately describe the constraint effect of congested

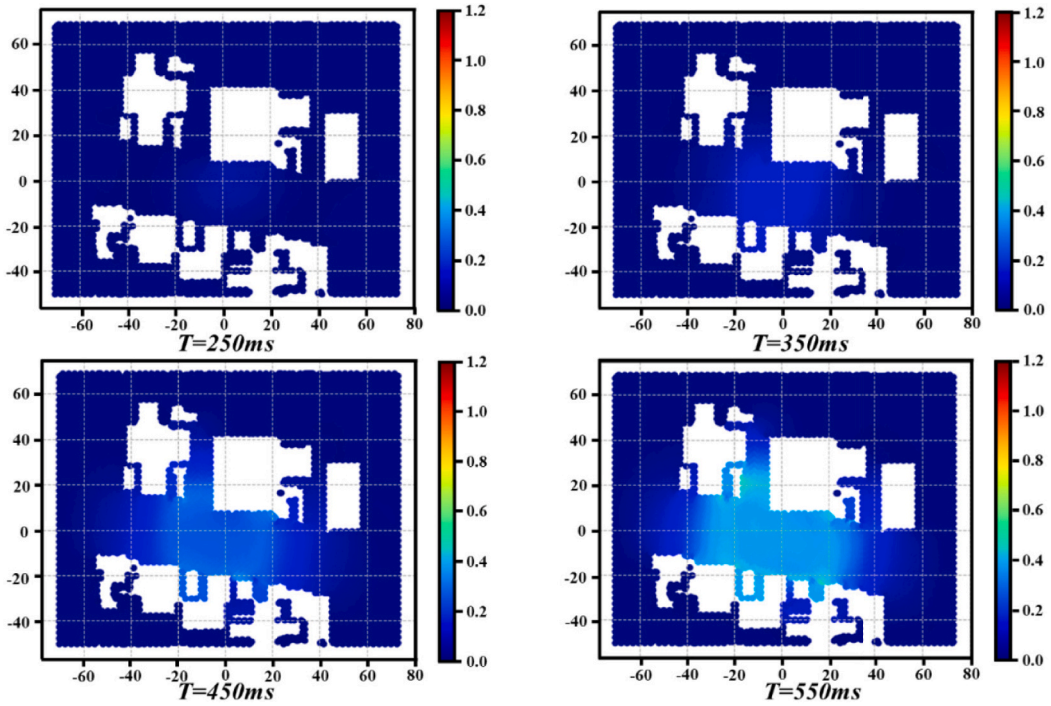

c) Transformer approach

Fig. 9. (*continued*).

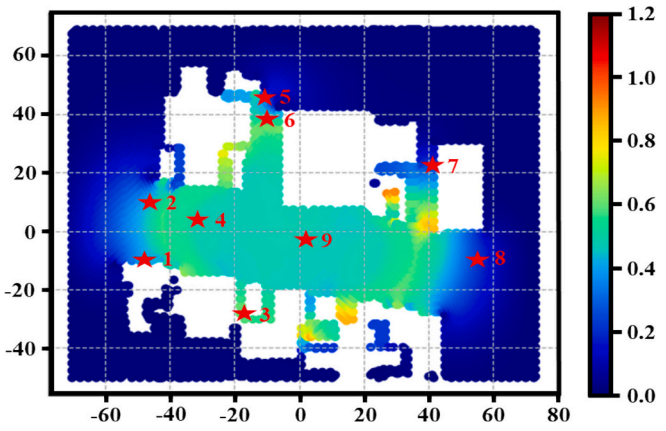

Fig. 10. Different positions randomly selected from the main road, constraint areas between two buildings.

buildings on blast wave propagation.

Fig. 11 demonstrates the comparison of predicted maximum overpressures at 9 different positions. These positions are randomly selected from the main road, constraint areas between two buildings as is shown in Fig. 10. From it, one may see the points 1, 2 5, 6,7 and 8 are localized at the edge of the urban block and the point 3 is selected between two congested buildings. These points are used to check the prediction accuracy of maximum overpressures by each approach after a long-distance interaction of blast wave with congested buildings. In addition, the points 4 and 9 are closed to the ignition position, indicating less congested buildings affecting the blast wave propagation. From Fig. 11, one may see most of the maximum overpressure predicted by our GNN approach are located between ±25 % error intervals even though a large prediction error still exists at the point 8. Nevertheless, this prediction error by our GNN approach is smaller than that by both MLP and Transformer approaches. In addition, both MLP and Transformer approaches has the prediction errors larger than 25 % at the points 1, 2, 7 and 8. This may be attributed that both approaches have poor performance to capture the long-distance interaction between congested buildings and blast wave propagation. Furthermore, the Transformer approach gives the predictions far away from the ±25 % error intervals at the points 5 and 6, further indicating its poor performance of maximum overpressures prediction at the congested urban area. Also, the MLP approach gives the worse prediction at the point 9, indicating its low accuracy to capture the dynamics of gas explosion not only at the congested area but also in the air. This is corresponding to the phenomena concluded in the reference [30].

Table 2 demonstrates comparison of R^2 and *MSE* between GNN, MLP and Transformer approaches. Please noting that both R^2 and *MSE* values are determined by using all the simulation data from testing dataset. From it, one may see our developed GNN approach has a highest R^2 value of 0.8860 and a lowest *MSE* value of 7.36E-4 compared to MLP and Transformer approaches. In addition, our proposed GNN approach exhibits a real-time capability with inference time of 16.13 ms for this large-scale spatiotemporal overpressure prediction of gas explosion with congested buildings. The integration of GIS with GNN has the 1000× computational speedup improvement compared to the integration of GIS with CFD, which requires 2 h for the urban-scale gas explosion prediction. Overall, the above results verify the more accuracy of our proposed GNN approach compared to MLP and Transformer approaches, and its highly computational efficiency compared to CFD approach in terms of gas explosion prediction with congested buildings at urban scale.

6. Discussions

Although exhibiting the higher accuracy as well as the real-time capability of the proposed GNN approach in terms of the worst-case consequence of gas explosion at urban scale compared to the state-of-the-art models, the limitations still exist:

Firstly, the study did not consider the dynamic, time-varying nature of the initial LNG release and dispersion, which is a crucial precursor to

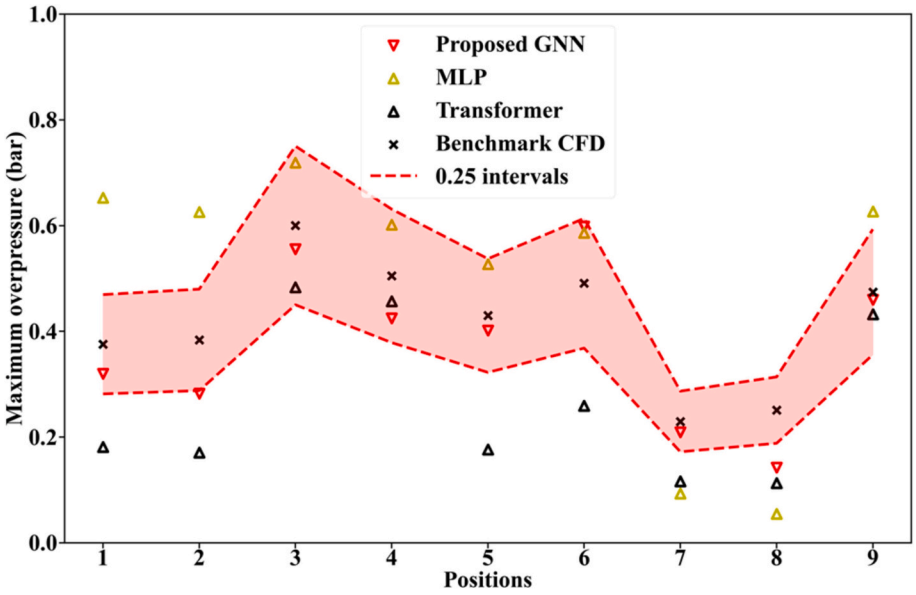

Fig. 11. Comparison of predicted maximum overpressures at different positions randomly selected.

Table 2
Comparison of R^2 and *MSE* between GNN, MLP and Transformer approaches.

Model	R^2	*MSE*	Inference time
GNN	0.9460	5.36E-4	16.13 ms
MLP[43]	0.5693	2.57E-3	15.62 ms
Transformer [44]	0.7368	1.36E-3	31.24 ms
CFD	//	//	2 h

the subsequent gas explosion modeling. The factors influencing the size and growth of the flammable vapor cloud, such as leak size, shut-off time, and ignition delay, can significantly impact the eventual explosion consequences at the urban scale. Instead, the study applied a conservative approach by assuming the potentially largest volume of the flammable vapor cloud, based on published research [31,32]. This conservative assumption allows the developed GNN model to assess the worst-case consequences of the gas explosion, while may not accurately capturing the time-varied nature of the incident. Further work is needed to integrate the time-varying release and dispersion process, along with the associated turbulence conditions, into the GNN model development to provide a more comprehensive and realistic assessment. The expected solution includes for example, *1]* Incorporate the gas release and dispersion simulation as an integral part of the modeling, rather than using a separate conservative approach. *2]* Capture the time-varying characteristics of the vapor cloud, including its volume, concentration, and turbulence conditions. *3]*Use the dynamic input from the release and dispersion simulation to drive the gas explosion modeling and prediction as well as the deep learning modeling procedure.

Secondly, the developed GNN model was focused on predicting the maximum overpressure values at different locations, rather than the full time-varying overpressure profiles, for the purpose of assessing the worst-case destructive effects on urban structures. The maximum overpressure is generally the most critical parameter for evaluating the conservative, worst-case scenario impacts, even if predicting the full overpressure-time histories would be more accurate for assessing the dynamic structural effects. The trade-off between computational efficiency, conservatism, and accuracy is a reasonable justification for the model's design choices. During this research work, the authors recognized that the lower accuracy of the pressure-time profile prediction, especially near congested buildings, is a limitation of the current GNN model. Future work is also expected to enhance the pressure-time profile predictions of this GNN model at urban scale by for example integrating prior knowledge on flame propagation or using physics-based constraints.

Lastly, several empirical and analytical models, such as the TNO multi-energy method and the Baker-Strehlow-Tang (BST) method, have been developed and validated for predicting gas explosions in congested environments. These models are integrated into industrial software frameworks, commonly used in quantitative risk assessments (QRA). This study did not compare the developed GNN model with these physics-based models. In contrast, this research emphasizes a data-driven approach through the development of an innovative GNN-based prediction model, which diverges from traditional physics-based principles. The primary advantage of this data-driven method lies in its ability to learn the underlying relationships of blast wave evolution as it interacts with urban structures, without requiring prior knowledge of physical or critical conditions, such as strong shock wave interactions. Nonetheless, the authors acknowledge that this approach has limitations. Specifically, the GNN model is applicable only to the urban environment for which it was trained. Any changes in the environment would necessitate retraining and validation of a new GNN model. To address this issue, the authors are actively exploring methods to enhance the generalization of the GNN model across various urban environments, including adapting to different building layouts by integrating physics with the data-driven training process.

7. Conclusions

This study developed an integrated approach of Geographic information systems (GIS) and graph neural network (GNN) for real-time obstructed gas explosion prediction at urban scale. In this approach, GIS provides 3D building geometries and grid information at urban scale. GNN approach solves the interaction between urban buildings and blast wave propagation. Comparison with the state-of-the-art approaches of gas explosion prediction was conducted. The results demonstrated that:

(1) The training process of GNN approach without considering the graph nodes inside these buildings contributes to describing the interaction between congested buildings and blast wave propagation more accurately.

(2) The proposed approach exhibits R^2 of 0.946 and *MSE* of 5.36E-4, indicating its higher prediction accuracy for blast load evolution especially at the congested building areas compared to the state-of-the-arts, i.e., MLP and Transformer approaches.
(3) The proposed approach exhibits a competitive real-time capability with inference time less than 1 s compared to the state-of-the-arts, i.e., MLP and Transformer approaches. However, it has the 1000× computational speedup improvement compared to the CFD approach at urban scale.
(4) This developed approach has the potential to accurately and quickly assess the worst-case destructive effects of gas explosion at urban scale, supporting the decision-makings about urban planning to improve urban resilience in the context of urban energy transition.

CRediT authorship contribution statement

Jihao Shi: Investigation, Project administration, Methodology, Formal analysis, Validation. **Junjie Li:** Resouces, Data curation, Validation. **Haoran Zhang:** Project administration, Methodology, Investigation, Funding acquisition. **Bin Xie:** Validation, Supervision. **Zonghao Xie:** Formal analysis, Data curation. **Qing Yu:** Resources, Project administration. **Jinyue Yan:** Resources, Project administration.

Declaration of competing interest

The authors declare the following financial interests/personal relationships which may be considered as potential competing interests: Jihao Shi, Junjie Li, Haoran Zhang, Bin Xie, Zonghao Xie, Yu Qing, and Jinyue Yan declare that they have no known competing financial interests or personal relationships that could have appeared to influence the work reported in this paper. This manuscript has not been published and is not under consideration for publication elsewhere. There are no conflicts of interest to disclose. Haoran Zhang, as the corresponding author, has ensured that all authors have read and approved the final version of the manuscript being submitted. The authors have agreed to the submission policies of the journal. All data generated or analyzed during this study are included in this published article. The authors confirm that the content of the manuscript has not been published, or submitted for publication elsewhere. If any financial support has been provided for the research, it should be disclosed here. Any involvement of study sponsors in the study design; collection, analysis, and interpretation of data; writing of the report; or the decision to submit the report for publication, if any, should be declared in this section.

Data availability

No data was used for the research described in the article.

Acknowledgments

This study was supported by National Natural Science Foundation of China (Project No.: 52101341). The authors would like to acknowledge partially support of the Hong Kong Research Grants Council (T22-505/19-N). The authors also much appreciate the guidance and help about GNN algorithm development from Dr. Qilin Li from Curtin University (Australia).

Appendix A. MLP's architecture

Parts	Layers
Input layers	9723 explosion overpressure values
Hidden layers	256, fully-connected neural network, Mish 256, fully-connected neural network, Mish 256, fully-connected neural network, Mish
Output layers	9723, fully-connected neural network, Softplus

Transformer's architecture.

Parts	Layers
Feature tokenizers	9723, Linear projection, none
Transformer Layers	192 tokens, Transformer module, ReLU 192 tokens, Transformer module, ReLU 192 tokens, Transformer module, ReLU 192 tokens, Transformer module, ReLU
Prediction Head	9723, fully-connected neural network, ReLU
Noting that Transformer module consists of 2 layers of Multi-Head Self-Attention and LayerNorm.	

GNN's architecture.

Parts	Layers
Encoder	1, MLP blocks for node 1, MLP blocks for edge
Processor	5, GraphNet blocks for graph
Decoder	1, MLP blocks for node 1, MLP blocks for edge
Noting that the MLP block consists of 4 layers of fully-connected neural networks with 64 neurons, in which the front 3 layers apply RuLU activation function and the last apply Linear activation function. GraphNet block consists of MLP block for node operation and MLP block for edge operation.	

MLP's optimization hyper-parameters.

Hyper-parameter	
Optimizer	Cosine annealing
Learning rate ranges	1e-3 to 10–6
Batch size	4
Dropout rate	0.06
Loss function	MSE
Training epochs	150,000

Transformer's optimization hyper-parameters.

Hyper-parameter	
Token dimensions	192
Attention heads	8
Optimizer	Cosine annealing
Learning rate ranges	1e-3 to 10–6
Batch size	4
Dropout rate	0.1
Loss function	MSE
Training epochs	150,000

GNN's optimization hyper-parameters.

Hyper-parameter	
Optimizer	Cosine annealing
Learning rate ranges	1e-3 to 10–6
Batch size	4
Loss function	MSE
Training epochs	150,000

Appendix B. Supplementary data

Supplementary data to this article can be found online at https://doi.org/10.1016/j.apenergy.2024.124614.

References

[1] Al-Orabi AM, Osman MG, Sedhom BE. Analysis of the economic and technological viability of producing green hydrogen with renewable energy sources in a variety of climates to reduce CO2 emissions: a case study in Egypt. Appl Energy 2023;338:120958.

[2] Sharifi A, Allam Z, Bibri SE, Khavarian-Garmsir AR. Smart cities and sustainable development goals (SDGs): a systematic literature review of co-benefits and trade-offs. Cities 2024;146:104659.

[3] Chen P. Urban planning policy and clean energy development harmony-evidence from smart city pilot policy in China. Renew Energy 2023;210:251–7.

[4] Ulpiani G, Vetters N, Shtjefni D, Kakoulaki G, Taylor N. Let's hear it from the cities: on the role of renewable energy in reaching climate neutrality in urban Europe. Renew Sustain Energy Rev 2023;183:113444.

[5] He T, Chong ZR, Zheng J, Ju Y, Linga P. LNG cold energy utilization: prospects and challenges. Energy 2019;170:557–68.

[6] Hermesmann M, Tsiklios C, Müller T. The environmental impact of renewable hydrogen supply chains: local vs. remote production and long-distance hydrogen transport. Appl Energy 2023;351:121920.

[7] Østergaard PA, Duic N, Noorollahi Y, Kalogirou S. Advances in renewable energy for sustainable development. Renew Energy 2023;219:119377.

[8] Rafique MM, Rehman S, Alhems LM. Developing zero energy and sustainable villages–a case study for communities of the future. Renew Energy 2018;127:565–74.

[9] Giannissi S, Venetsanos A. Study of key parameters in modeling liquid hydrogen release and dispersion in open environment. Int J Hydrogen Energy 2018;43(1):455–67.

[10] Cleaver P, Johnson M, Ho B. A summary of some experimental data on LNG safety. J Hazard Mater 2007;140(3):429–38.

[11] Tsinghua. A gas explosion occurred at Fuyang BBQ restaurant in Yinchuan City, Ningxia, killing 31 people and injuring 7 people. Safety Security Office Tsinghua Univ 2023. June 23. Available from: https://peace.tsinghua.edu.cn/info/1022/2023.htm.

[12] Daily KJ. Gas explosion in Pyeongchang: Korea JoongAng Daily [cited 2024 2024, January 2]. Available from: https://koreajoongangdaily.joins.com/news/2024-01-02/national/socialAffairs/Gas-explosion-in-Pyeongchang/1949310; 2024.

[13] Luketa-Hanlin A, Koopman RP, Ermak DL. On the application of computational fluid dynamics codes for liquefied natural gas dispersion. J Hazard Mater 2007;140(3):504–17.

[14] Zhao X, Chen C, Shi C, Chen J, Chen Q, Zhao D. A three-dimensional simulation of the effects of obstacle blockage ratio on the explosion wave in a tunnel. J Thermal Anal Calorimetry 2021;143:3245–56.

[15] Wang K, Shi T, He Y, Li M, Qian X. Case analysis and CFD numerical study on gas explosion and damage processing caused by aging urban subsurface pipeline failures. Eng Failure Anal 2019;97:201–19.

[16] Švec P, Skřínský J. APPLICATION OF GIS FOR THE CONTROL OF MAJOR ACCIDENT HAZARDS. Geo Sci Eng 2022;68(2).

[17] Ma G, Huang Y. Safety assessment of explosions during gas stations refilling process. J Loss Prevention Process Ind 2019;60:133–44.

[18] Li F, He X, Zhang Y, Wang C, Tang J, Sun R. Superposition risk assessment of the working position of gas explosions in chinese coal mines. Process Safety Environ Protect 2022;167:274–83.

[19] Mohr L, Benauer R, Leitl P, Fraundorfer F. Damage estimation of explosions in urban environments by simulation. Int Archives Photogrammetry, Remote Sensing and Spatial Information Sciences-ISPRS Archives 2019;42(W8):253–60.

[20] Chen W, Su H, Yong Y, Hu Z. Decision support system for urban major hazard installations management based on 3DGIS. Physics Chem Earth, Parts A/B/C 2019;110:203–10.

[21] Taud H, Mas J. Multilayer perceptron (MLP). Geomatic approaches for modeling land change scenarios. 2018. p. 451–5.

[22] Xu Q, Chen G, Su S, Men J, Li G. Prediction of venting gas explosion overpressure based on a combination of explosive theory and machine learning. Expert Systems Appl 2023;234:121044.

[23] Zhang RH. A study on overpressure prediction of vapor cloud explosion based on bp artificial neural network. J Eng Des 2010;5(17(3)).

[24] Shi J, Zhang H, Li J, Xie W, Zhao W, Usmani AS, et al. Real-time natural gas explosion modeling of offshore platforms by using deep learning probability approach. Ocean Eng 2023;276:114244.

[25] Li Q, Wang Y, Li L, Hao H, Wang R, Li J. Prediction of BLEVE loads on structures using machine learning and CFD. Process Safety Environ Protection 2023;171:914–25.

[26] Scarselli F, Gori M, Tsoi AC, Hagenbuchner M, Monfardini G. The graph neural network model. IEEE Trans Neural Netw 2008;20(1):61–80.

[27] Battaglia PW, Hamrick JB, Bapst V, Sanchez-Gonzalez A, Zambaldi V, Malinowski M, et al. Relational inductive biases, deep learning, and graph networks. arXiv preprint arXiv:180601261. 2018.
[28] Sanchez-Gonzalez A, Godwin J, Pfaff T, Ying R, Leskovec J, Battaglia P. Learning to simulate complex physics with graph networks. Int Conf Mach Learning 2020;119:8459–68. PMLR.
[29] Belbute-Peres FDA, Economon T, Kolter Z. Combining differentiable PDE solvers and graph neural networks for fluid flow prediction. Int Conf Mach Learning 2020;119:2402–11. PMLR.
[30] Li Q, Wang Y, Chen W, Li L, Hao H. Machine learning prediction of BLEVE loading with graph neural networks. Reliability Eng System Safety 2024:241. https://doi.org/10.1016/j.ress.2023.109639.
[31] Giannissi S, Venetsanos A. A comparative CFD assessment study of cryogenic hydrogen and LNG dispersion. Int J Hydrogen Energy 2019;44(17):9018–30.
[32] Hansen OR, Gavelli F, Ichard M, Davis SG. Validation of FLACS against experimental data sets from the model evaluation database for LNG vapor dispersion. J Loss Prevention Process Ind 2010;23(6):857–77.
[33] Li Q, Wang Y, Chen W, Li L, Hao H. Machine learning prediction of BLEVE loading with graph neural networks. Reliability Eng System Safety 2024;241:109639.
[34] Loshchilov I, Hutter F. Decoupled weight decay regularization. arXiv preprint arXiv:171105101. 2017.
[35] Pfaff T, Fortunato M, Sanchez-Gonzalez A, Battaglia PW. Learning mesh-based simulation with graph networks. arXiv preprint arXiv:201003409. 2020.
[36] Han X, Gao H, Pfaff T, Wang J-X, Liu L-P. Predicting physics in mesh-reduced space with temporal attention. arXiv preprint arXiv:220109113. 2022.
[37] Hansen OR, Johnson DM. Improved far-field blast predictions from fast deflagrations, DDTs and detonations of vapour clouds using FLACS CFD. J Loss Prevention Process Ind 2015;35:293–306.
[38] Pedersen H, Tomlin G, Middha P, Phylaktou H, Andrews G. Modelling large-scale vented gas explosions in a twin-compartment enclosure. J Loss Prevention Process Ind 2013;26(6):1604–15.
[39] Yang Y, Yang S, Fang Q, Xiang H, Sun W, Liu X. Large-scale experimental and simulation study on gas explosion venting load characteristics of urban shallow buried pipe trenches. Tunnelling Underground Space Technol 2022;123:104409.
[40] Lucas M, Atanga G, Hisken H, Mauri L, Skjold T. Simulating vented hydrogen deflagrations: improved modelling in the CFD tool FLACS-hydrogen. Int J Hydrogen Energy 2021;46(23):12464–73.
[41] Li J, Hao H. Numerical and analytical prediction of pressure and impulse from vented gas explosion in large cylindrical tanks. Process Safety Environ Protect 2019;127:226–44.
[42] GexCon. FLACS v10.4 User's manual. Norway: Doxygen; 2015.
[43] Li J, Li Q, Hao H, Li L. Prediction of BLEVE blast loading using CFD and artificial neural network. Process Safety Environ Protect 2021;149:711–23.
[44] Li Q, Wang Y, Shao Y, Li L, Hao H. A comparative study on the most effective machine learning model for blast loading prediction: from GBDT to transformer. Eng Struct 2023;276:115310.
[45] Zhang X, Shi J, Li J, Huang X, Xiao F, Wang Q, Chen G. Hydrogen jet and diffusion modeling by physics-informed graph neural network. Renew. Sust. Energy Rev. 2025;207:114898.